Thick Liquid-Walled Spheromak Magnetic Fusion Power Plant

R.W. Moir, R.H. Bulmer, T.K. Fowler, T.D. Rognlien, M.Z. Youssef

April 8, 2002

DISCLAIMER

This report has been reproduced directly from the best available copy.

Available electronically at http://www.doc.gov/bridge

Available for a processing fee to U.S. Department of Energy
And its contractors in paper from
U.S. Department of Energy
Office of Scientific and Technical Information
P.O. Box 62
Oak Ridge, TN 37831-0062
Telephone: (865) 576-8401
Facsimile: (865) 576-5728
E-mail: reports@adonis.osti.gov

Available for the sale to the public from
U.S. Department of Commerce
National Technical Information Service
5285 Port Royal Road
Springfield, VA 22161
Telephone: (800) 553-6847
Facsimile: (703) 605-6900
E-mail: orders@ntis.fedworld.gov
Online ordering: http://www.ntis.gov/ordering.htm

OR

Lawrence Livermore National Laboratory
Technical Information Department's Digital Library
http://www.llnl.gov/tid/Library.html

Thick liquid-walled spheromak magnetic fusion power plant

R. W. Moir, R. H. Bulmer, T. K. Fowler, T. D. Rognlien, M. Z. Youssef

April 8, 2002

Abstract

We assume a spheromak configuration can be made and sustained by a steady gun current, which injects particles, current and magnetic field, i.e., helicity injection. The equilibrium is calculated with an MHD equilibrium code, where an average beta of 10% is found. The toroidal current of 40 MA is sustained by an injection current of 100 kA (125 MW of gun power). The flux linking the gun is $1/1000^{th}$ that of the flux in the spheromak. The geometry allows a flow of liquid, either molten salt, (flibe–Li_2BeF_4 or flinabe–$LiNaBeF_4$) or liquid metal such as SnLi which protects most of the walls and structures from neutron damage. The free surface between the liquid and the burning plasma is heated by bremsstrahlung and optical radiation and neutrons from the plasma. The temperature of the free surface of the liquid is calculated and then the evaporation rate is estimated. The impurity concentration in the burning plasma is estimated and limited to a 20% reduction in the fusion power. For a high radiating edge plasma, the divertor power density of 460 MW/m^2 is handled by high-speed (20 m/s), liquid jets. For low radiating edge plasmas, the divertor-power density of 1860 MW/m^2 is too high to handle for flibe but possibly acceptable for SnLi with jets of 100 m/s flow speed. Calculations show the tritium breeding is adequate with enriched ^{6}Li and appropriate design of the walls not covered by flowing liquid 15% of the total). We have come up with a number of problem areas needing further study to make the design self consistent and workable.

Table of contents

Introduction and background

This power plant design study applies liquid walls to the steady state spheromak plasma confinement configuration. A self-consistent point design was not achieved in all aspects due to known inconsistencies. These inconsistencies set the agenda for further work.

The spheromak idea came about by a number of routes[1]. The toroidal coils of the tokamak might not be necessary if the plasma could carry enough current in the toroidal direction to make a sufficient toroidal field. In this case, the performance might be tokamak-like with a simpler magnet configuration. Marshall plasma guns made reasonably stable configurations. Early experiments were encouraging. Hagenson and Krakowski made a reactor design [2]. Other reactor studies included solid first walls and boiling liquid blankets [3] and pulsed liquid walls [4]. The main theme of this work is the use of liquid wall and steady state operation.

The logic of this design process follows:
- the configuration is description based on MHD equilibrium calculations
- a discussion of the steady-state gun injection for current drive
- the development of the plasma and other related parameters
- a discussion of the electrodes and insulators
- a discussion of the liquid wall flows with the calculation of surface temperatures (based on incident power on the liquid surface and interior,)
- the calculation of evaporation rates from the liquid surfaces that depend only on surface temperature
- discussion of the edge plasma, the estimates of evaporation allowed from core plasma contamination with impurities, and the ability to breed tritium

We consider low conductivity liquids (molten salts) and high conductivity liquids (liquid metals). The usual molten salt is flibe (Li_2BeF_4), but past studies

show the evaporation limits require temperatures near or below the melt temperature of 460 °C. Adding NaF to flibe produces flinabe (NaF+LiF+BeF$_2$ = LiNaBeF$_4$),[5], whose melt temperature is reduced to ~310 °C. This study is based on flinabe as a candidate molten salt. SnLi is the liquid metal candidate.

There are many aspects of the design that do not meet requirements or are inconsistent. These are discussed through out the report and many suggestions for further work are made.

Configuration-equilibria

The spheromak reactor shown in Fig. 1 was developed with the Corsica code. It is an axi-symmetric configuration with a nearly up/down symmetric confined region, but with slight vertical asymmetry to provide a single (lower) divertor. The shape of the confined region is maintained with 6 circular coils arranged in an up/down symmetric fashion. Two additional coils channel diverted flux around the gun electrodes and into a collector region. The free-boundary equilibrium is designed to have a flux amplification factor of 1000 with an elongation less than 2 to mitigate instabilities. Of particular concern are tilt and shift modes which will probably require [6] active feedback coils. These coils are envisioned to be relatively small and located near the inner surface of the . shielding structure facing the plasma in the confined region. The outer radius of the confined region is 6 m and the confined volume is 652 m^3.

The distance from the outer edge of the plasma to the first conducting wall is 1 m in the case of flibe (0.5 m from the plasma edge to the low conductivity flibe and 0.5 m of flibe to the 30 mm thick stainless steel wall). In the case of SnLi the conducting liquid wall is 0.5 m away from the plasma.

Retractable electrode

Shield

SR01004

16

14

Inlet nozzle

Top tritium breeding blanket

12

Flowing liquid

Free surface

10

Secondary (inactive) separatrix

8

6

Superconducting magnets

Thick ~30 mm structure

Radial thick liquid wall/ blanket

2

0

-2

-4

Separatrix/ plasma edge

Thin ~3 mm flow divider

Bottom breeding blanket

-6

-8

Shields

-10

Jet/ droplet divertor

-12

Slow liquid flow

-14

Outlet nozzle

-16

-10 -8 -6 -4 -2 0 2 4 6 8 10

3/20/2002

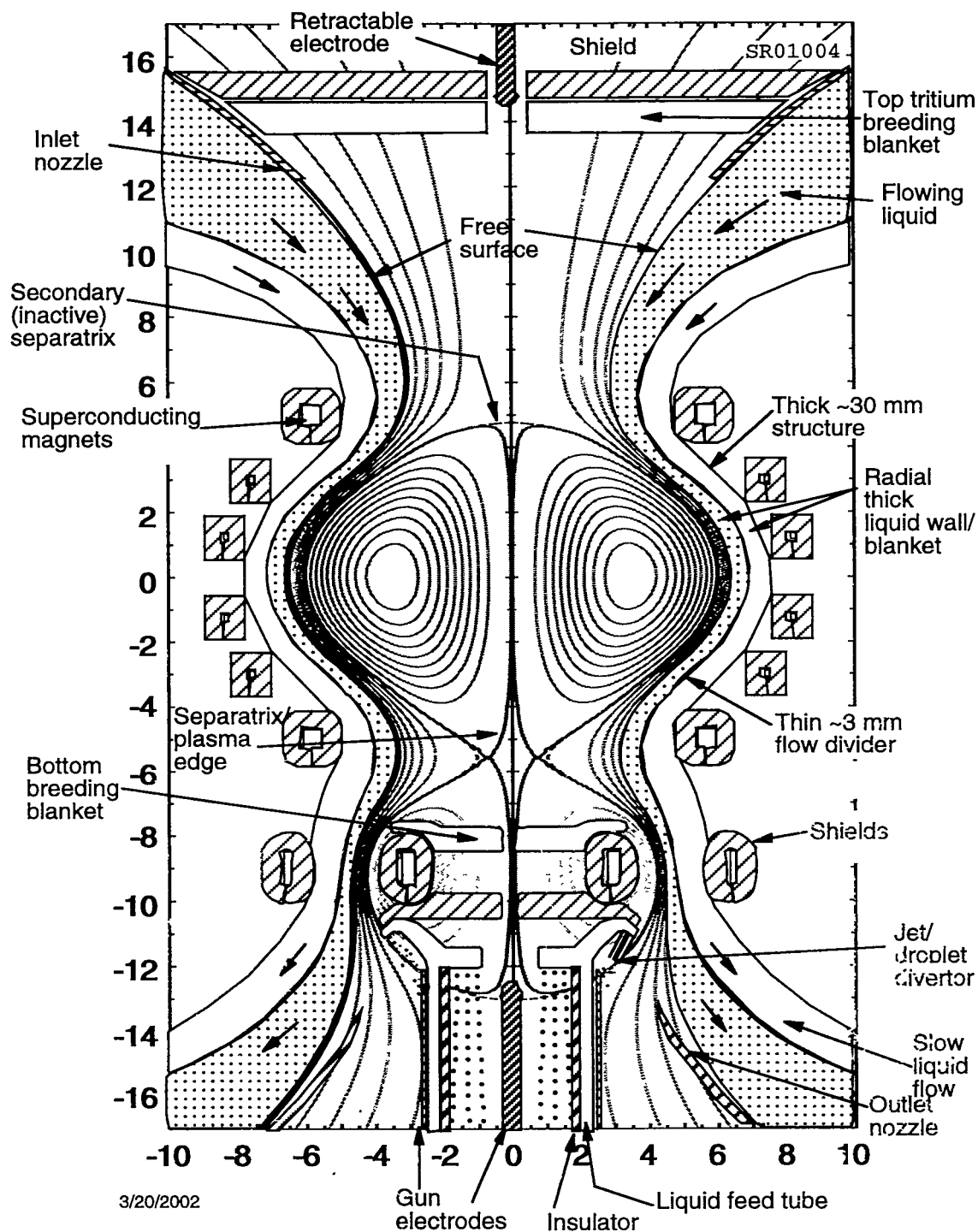Gun electrodes

Liquid feed tube

Insulator

Fig. 1. The spheromak configuration with liquid walls shown above is the subject of this report. The liquid flow is kept to the outside by centrifugal force for molten salt and by magnetic guide field for liquid metals. Liquid jets greatly aid divertor heat removal.

The current profile deviates from the relaxed Taylor-state in that the λ–profile (normalized current density, see [1]):

$$\lambda(\psi) = \frac{\mu_0 \mathbf{j} \cdot \mathbf{B}}{B^2} \qquad (1)$$

varies as shown in Fig. 2, creating shear consistent with a Mercier beta limit of 10%. The value of λ on the open field-lines is about half that at the magnetic axis. The pressure profile, as shown also shown in Fig.2, has been optimized to yield the maximum Mercier limit for the given λ–profile. The q-profile varies from 0.9 on the magnetic axis to 0.3 near the edge.

The toroidal current is 40 MA which results in $B_\varphi \approx B_\theta = 2.89$ T at the magnetic axis[1] (magnetic field profiles are shown in Fig. 3). This level of current requires pack current densities of ~30 A/mm^2 in the shaping coils (near a practical limit) with the sizes as shown in Fig. 1. As noted, the toroidal current will have to increase as the design evolves, with the coil currents increasing in direct proportion. Therefore, the coil cross-sectional dimensions will have to increase by about 25% to keep the current densities within limits.

The main equilibrium parameters are summarized in Table 1. Note the gun current in the equilibrium model, 18.2 kA, is significantly less than the 100 kA value discussed in the gun model section later on. This discrepancy is due to the particular values of the toroidal current and the ratio of λ_{ext}/λ_0 used in the equilibrium model, and needs to be resolved as the design evolves.

Another area for future work involves the edge-flux expansion ratio from the midplane to the divertor region. In the present design, the radial distance between the edge of the confined region and the inactive separatrix ($\Psi=0$

contour) is 1.5 mm and only expands by a factor of 4 to 6 mm in the divertor region. This expansion ratio needs to increase by a factor of 2 to 12 mm in the divertor region to be able to handle the power flux density discussed in the divertor section. This change will require an adjustment in the current and in the position of the outer divertor coil. Perhaps it will also require an additional divertor coil.

Table 1

Equilibrium parameters

Toroidal current, MA	40
Toroidal B-field (axis), T	2.89
Poloidal current (gun), kA	18.2
Poloidal B-field (R=0), T	5.24
Poloidal flux (edge), Wb (r=0 to separatrix)	0.08
Poloidal flux (axis), Wb	75.8
Separatrix radius, inner, m	0.068
Separatrix radius, outer, m	6.00
Magnetic axis radius, m	3.49
Core plasma volume, m^3	652
Core plasma surface, m^2	362
Volume average beta, %	10

---

[1] This field level is not yet consistent with the total fusion power. The toroidal current will have to be increased to ~60 MA to produce the desired 4.3 T field level if this is the correct field to scale from (see the next section for a discussion of scaling and further work needed).
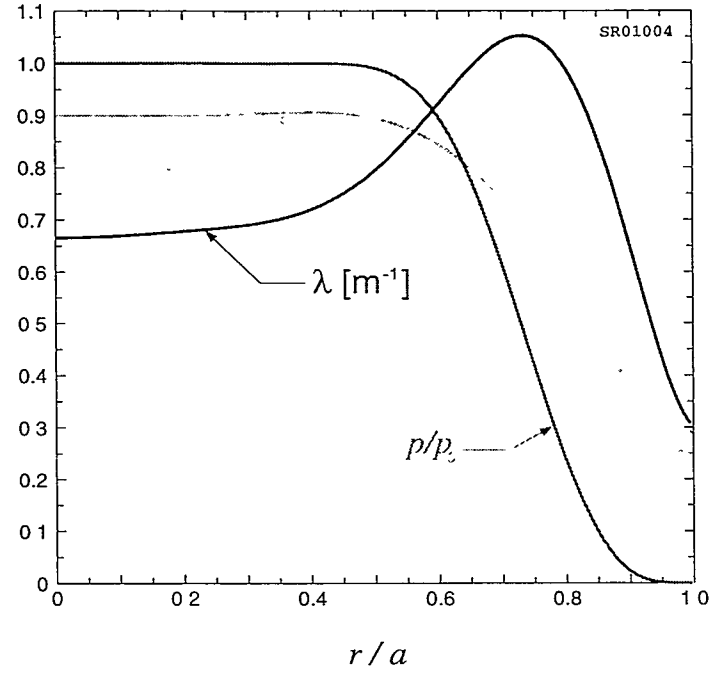
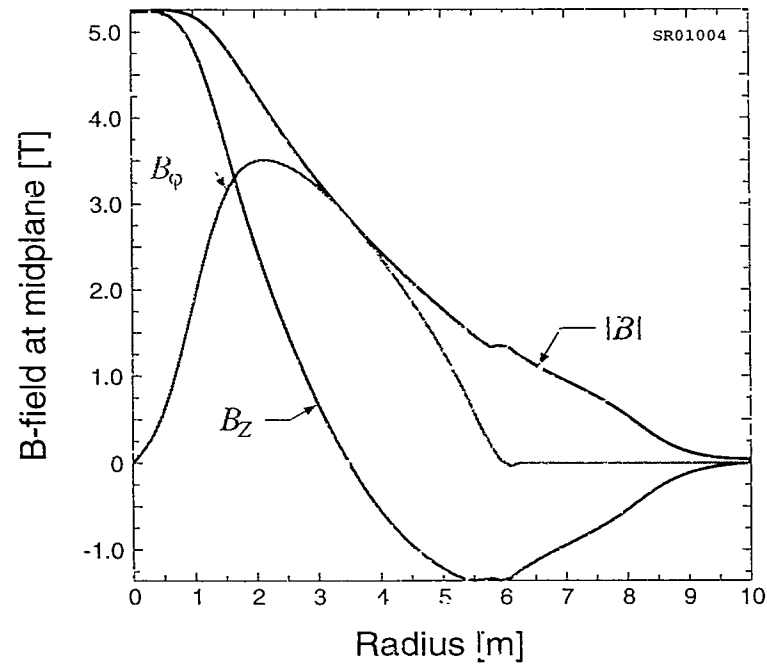Fig. 2. Profiles of pressure, current (λ) and Safety Factor (q) at the midplane.

Fig. 3. Magnetic field profile. The field is consistent with a model having 40 MA toroidal current and beta equal to 10% volume averaged

8

Plasma parameters

The Corsica model has a plasma pressure such that the volume averaged beta is 10%. The field of 5.24 T on r=0 axis, which corresponds to a 40 MA toroidal current. Based on prior work on the Field Reversed Configuration (FRC) [7], we can scale to get a first approximation of some of the parameters. First we scale the power density.

$$\frac{P_{FRC}}{V} = \frac{2500}{2.6} = 961.5 \frac{MW}{m^3} \qquad \text{r=0.39 m separatrix case for FRC for scaling} \qquad (2)$$

$$\frac{P_{Spheromak}}{V} = \frac{2500}{652} = 3.834 \frac{MW}{m^3} \qquad (3)$$

$$\frac{P}{V} \propto n^2 \propto \frac{\beta^2 B^4}{T^2} \qquad (4)$$

$$\frac{(\beta^2 B^4)_{Sph}}{(\beta^2 B^4)_{FRC}} = \frac{3.834}{961.5} = 3.988 \cdot 10^{-3} \qquad (5)$$

From Table 2 we see the FRC field is 5.5 T but this is on the r=0 axis (the field on the magnetic axis is zero for the FRC).

$$B_{Sph} = (3.988 \cdot 10^{-3} \cdot 0.97^2 \cdot 5.5^4 / 0.1^2)^{\frac{1}{4}} = 4.305 T \qquad (6)$$

This value of magnetic field probably corresponds to the value somewhere between the r=0 axis of 2.89 T and that at the magnetic axis of 5.24 T –a reasonable first guess. A better estimate is left to future work.

The plasma density is also scaled from the FRC work.

$$n_{Sph} \propto \frac{1}{\sqrt{\frac{P}{V}}} \qquad (7)$$

9

$$n_{Sph} = 26 \cdot 10^{20} \sqrt{\frac{3.834}{961.5}} = 1.64 \cdot 10^{20} \, / \, m^3 \qquad\qquad (8)$$

The volume within the last closed flux contour is 652 m^3. The circumference in the poloidal plane of the last flux contour is 24.3 m. The area within this contour in the poloidal plane is 37.9 m^2. The surface area from the separatrix to the upper apex along the inside or nearest the axis is about 23 m^2 and the area on the outside is 362 m^2. This may be useful in deciding how much leakage plasma should enter the divertor on the outside versus the inside. Using the area ratio suggests the inside plasma leakage is only 6% of the outside leakage. We need to estimate the width of plasma flow on the inside flux surface to estimate the power density there. If we can show the power density on the inside divertor is small. We need only treat the outside divertor (see section on divertor).

Table 2

Typical spheromak power plant parameters.

	Spheromak	FRC	FRC
Liquid wall radius, m	6.5	1.5	2.0
Separatrix radius, m	0.068, 6.0	0.39	1
Magnetic axis, m	3.49	0.29	0.75
Separatrix length, outside and inside, m	15, 10	8	8
Liquid flow path length, inlet nozzle exit nozzle, m	27	14	14
Core plasma volume, m^3	652	2.6	25
Outer plasma area, m^2	362	75	100
Average ion temperature, keV	12	12	18
Average ion density, $10^{20} \, m^{-3}$	1.65	26	6.2
Peak ion density, $10^{20} \, m^{-3}$	?	31	6.8
Z_{eff}	1.5	1.5	1.5
s = plasma radius/ average larmor radius	1100	7.5	26
Helicity current drive, kA / Helicity (Gun) power, MW	100 / 125	---	---
Toroidal current, MA	40		40
Volume-averaged beta	0.1	0.97	0.78
Magnetic field, T Poloidal / Toroidal	Bz=5.24 @r=0 / Bϕ=2.89@r=3.49	5.5	3.6
Flux from r=0 to the separatrix, Wb	0.08	---	---
Flux from separatrix to mag axis, Wb	75.8	---	---
Energy confinement time, s	?	0.08	0.33

11

Ash particle conf. time, s	?	0.16	0.65
Neutron wall load ave, MW/m^2	5.5	27	18
Surface heat load, MW/m^2	0.47	1.7	1.2
Neutron power, MW	2000	2000	1844
Bremsstrahlung radiation power, MW	46 MW, 0.13 MW/m^2	46	49
Line radiation, core @15% P_{alpha}, MW	75 MW, 0.21 MW/m^2	---	----
Line radiation, edge@ 10% P_{alpha}, MW	50 MW, 0.14 MW/m^2	78	69
Charged-particle transport power, MW	454	415	383
Input (Gun) power, MW	125 @ Q=20	40	40
Fusion power, MW	2500	2500	2306
Net electric power, MWe	1000	1000	1000

Current Drive Model

The magnetized Marshall gun used to create and sustain spheromaks can be represented by an electric circuit in which the helicity injection impedance is approximated by a resistor, R_s, giving a total gun impedance [8]:

$$R_{GUN} = (5T/I) + R_{FC} + R_s \qquad (9)$$

where I is the gun current; 5T is the approximate sheath voltage with temperature T (in eV) in the "flux core" that guides the gun bias flux and current along the geometric axis of the machine; and R_{FC} is the ohmic resistance in the

flux core. Only R_S is useful in sustaining the spheromak, with an efficiency f, giving as the requirement for steady state:

$$fI^2R_S \quad = \quad P_\Omega \quad = \quad E/\tau \quad = \quad 14\,\text{MW} \qquad (10)$$

where P_Ω is the ohmic dissipation of the spheromak with magnetic energy E and decay time τ that we estimate as E = 700 MJ and τ = 50 s for the parameters in Table 2. Finally, an optimum efficiency of f = 0.5 is obtained for a gun current given by [7,8]:

$$I \quad = \quad f^{-1}(5/R\mu_o)\psi \quad = \quad 100\,\text{kA} \qquad (11)$$

where 5/R is the lowest Taylor eigenvalue for flux conserver radius R = 6m for the design shown here and flux core ψ = 0.08 W (the flux between r=0 and the separatrix). Scaling from SSPX gives T = 50 eV and R_{FC} = 1.4 mΩ if we take an effective length $\approx$ R along the goemetric axis in the the confinement region where the magnetic field B is highest and the cross-sectional area of the flux core (= ψ/B) is smallest [8].

The above formulas give the gun parameters in Table 4, which in turn give those of Table 2.

Table 4.

Gun Parameters

Gun Current, I (kA)	100
Helicity injection impedance, R_S (mΩ)	2.8
Total gun impedance, R_{GUN} (mΩ)	6.7
Gun voltage, I R_{GUN} (V)	670
Power consumed by the gun, I^2R_{GUN} (MW)	67
Gun power supply power, P (MW)	125

To limit the gun power to 125 MW, giving the nominal fusion gain Q = 20 in Table 2, requires a total impedance P/I = 12.5 mΩ, calling for a not-unreasonable

13

d.c. power supply impedance 12.5 - 6.7 = 5.8 mΩ and an overall efficiency to sustain the spheromak = P_Ω/P = 14/125 = 11%.

The unknown physics resides in the helicity injection impedance R_S–the subject of ongoing research in SSPX. The required value R_S = 2.8 mΩ in Table 4 is consistent with an enhanced resistance model of SSPX results, giving [8]:

$$R_S \quad = \quad f(1 - f^2)(\alpha\beta)\, R_{FC} \quad = \quad 2.5 \text{ mΩ} \tag{12}$$

with f = 0.5 as above and $\alpha\beta$ = 4.8 to fix SSPX data [7]. The actual impedance may be higher, giving somewhat different bias flux and current, greater efficiency, and higher Q (e.g. $R_S \approx$ 10 mΩ in earlier CTX results at Los Alamos [9]). The larger question is whether the instability processes of magnetic tearing and reconnection–thought to underlie the helicity injection impedance characteristic of short pulse experiments to date (milliseconds)–will persist in steady state.

Electrode design

The electrodes shown at the bottom of Fig. 1 provides the 100 kA of helicity current drive. Its active area is a disk of about 0.25 m radius. This gives a current density of 50 A/cm^2. A tapered electrode could reduce this current density and might ease cooling

Insulator design

The insulator is a cylindrical sleeve of radius 2 m about 5 m long, shown near the bottom of Fig. 1. Its purpose is to prevent current from passing across the gap between the center electrode at r=0.25 m and the cylindrical electrode at r $\approx$ 2.2 m. The insulator is shielded from line-of-sight radiation. The neutrons and x-rays dose rate to the insulator from indirect radiation needs to be calculated to determine its lifetime.

Power plant considerations

In this section we discuss the power flows. We assume 2500 MW of fusion power. Of this, 2000 MW is in the form of 14 MeV neutrons. Nuclear reactions in the flinabe blanket are assumed to multiply this by 1.18, giving 2360 MW thermal power in the blanket. To this we add the incident power of the 500 MW from alpha energy which all gets into the flowing fluid either in the walls or in the divertor. Also we add the helicity injection power. We assume a $Q=P_{fusion}/P_{injection}=20$ case, so $P_{injection}$ =125 MW. The total power going into the flowing fluid is 2985 MW.

> 2360 MW nuclear power in the blanket
> 500 MW alpha power
> <u>125 MW</u> injection power
> 2985 MW total

The volumetric flow rate ($\dot{V}$) is given by the flow at 10 m/s at the midplane with a 0.5 m thickness. The flow in the divertor jets and the slow flow in the back of the blanket are small compared to this.

$$\dot{V} = AV = 2\pi r \Delta r v = 2\pi 6.5 \cdot 0.5 \cdot 10 = 204.2 \; m^3 / s \tag{13}$$

<u>For flibe:</u>

The mass flow rate (see Fig. 5) is:

$$\dot{m}_{blanket} = 2000 \, kg/m^3 \cdot 204.2 \, m^3/s = 4.084 \cdot 10^5 \; kg/s = \text{flow through blanket} \tag{14}$$

The temperature increase in the mixed flow from inlet to outlet is:

$$\Delta T_{blanket} = \frac{P}{C \dot{m}_{blanket}} = \frac{2985 \; MW}{2380 \; J \, kg^{-1} K^{-1} \cdot 4.084 \cdot 10^5 \, kg/s} = 3.071 K \tag{15}$$

Past studies suggest a 100 °C temperature drop in the coolant to and from the heat exchangers is acceptable from an economic standpoint. We desire lower temperatures and use only 50 °C to keep the surface temperature low. This assumption will result in a modest plant cost increase.

$$\dot{m}_{HX} = \frac{P}{C \Delta T} = \frac{2985 MW}{2380 \, J \, kg^{-1} K^{-1} 50 \, K} = 2.5084 \cdot 10^4 \, kg/s = \text{flow to heat exchanger} \quad (16)$$

Since the blanket flow rate is larger than the flow to the heat exchanger, a fraction of the flow will be bypassed to the heat exchanger.

$$\dot{m}_{bypass} = \dot{m}_{blanket} - \dot{m}_{HX} = 4.084 \cdot 10^5 \, kg/s - 2.5084 \cdot 10^4 \, kg/s = 3.833 \cdot 10^5 \, kg/s \quad (17)$$

The temperature of the flow to the heat exchanger is assumed to be 450 °C and 400 °C of the flow out. The melt temperature is estimated at 350 °C (perhaps as low as 310 °) for flinabe, giving a small margin (50 °C). Flibe has a melt temperature of 460 °C.

<u>For SnLi:</u>

The mass flow rate (see Fig. 5) is:

$$\dot{m}_{blanket} = 6000 \, kg/m^3 \cdot 204.2 \, m^3/s = 12.25 \cdot 10^5 \, kg/s = \text{flow through blanket} \quad (18)$$

The temperature increase in the mixed flow from inlet to outlet is: ·

$$\Delta T_{blanket} = \frac{P}{C \dot{m}_{blanket}} = \frac{2985 \, MW}{318.1 \, J \, kg^{-1} K^{-1} \cdot 12.25 \cdot 10^5 \, kg/s} = 7.659 \, K \quad (19)$$

$$\dot{m}_{HX} = \frac{P}{C \Delta T} = \frac{2985 MW}{318.1 J kg^{-1} K^{-1} 100 \, K} = 0.9384 \cdot 10^5 \, kg/s \quad (20)$$

Since the blanket flow rate is larger than the flow rate to the heat exchanger, a fraction of the flow will be bypassed to the heat exchanger.

$$\dot{m}_{bypass} = \dot{m}_{blanket} - \dot{m}_{HX} = 12.25 \cdot 10^5 \, kg/s - 0.9384 \cdot 10^5 \, kg/s = 11.31 \cdot 10^5 \, kg/s \quad (21)$$

<u>For Li:</u>

The mass flow rate (see Fig. 5) is:

$$\dot{m}_{blanket} = 485 \, kg/m^3 \cdot 204.2 \, m^3/s = 0.9904 \cdot 10^5 \, kg/s = \text{flow through blanket} \quad (22)$$

The temperature increase in the mixed flow from inlet to outlet is:

$$\Delta T_{blanket} = \frac{P}{C} = \frac{2985 \, MW}{4200 \, J \, kg^{-1} K^{-1} \cdot 0.9904 \cdot 10^5 \, kg/s} = 7.176 \, K \quad (23)$$

$$\dot{m}_{HX} = \frac{P}{C \Delta T} = \frac{2985 MW}{4200 \, J \, kg^{-1} K^{-1} 50 \, K} = 1.421 \cdot 10^4 \, kg/s \quad (24)$$

Since the blanket flow rate is larger than the flow rate to the heat exchanger, a fraction of the flow will be bypassed to the heat exchanger.

$$\dot{m}_{bypass} = \dot{m}_{blanket} - \dot{m}_{HX} = 0.99037 \cdot 10^5 \ kg/s - 1.421 \cdot 10^4 \ kg/s = 8.482 \cdot 10^4 \ kg/s \qquad (25)$$

Cool liquid from the heat exchanger can be fed to the first wall or mixed with the bulk flow.
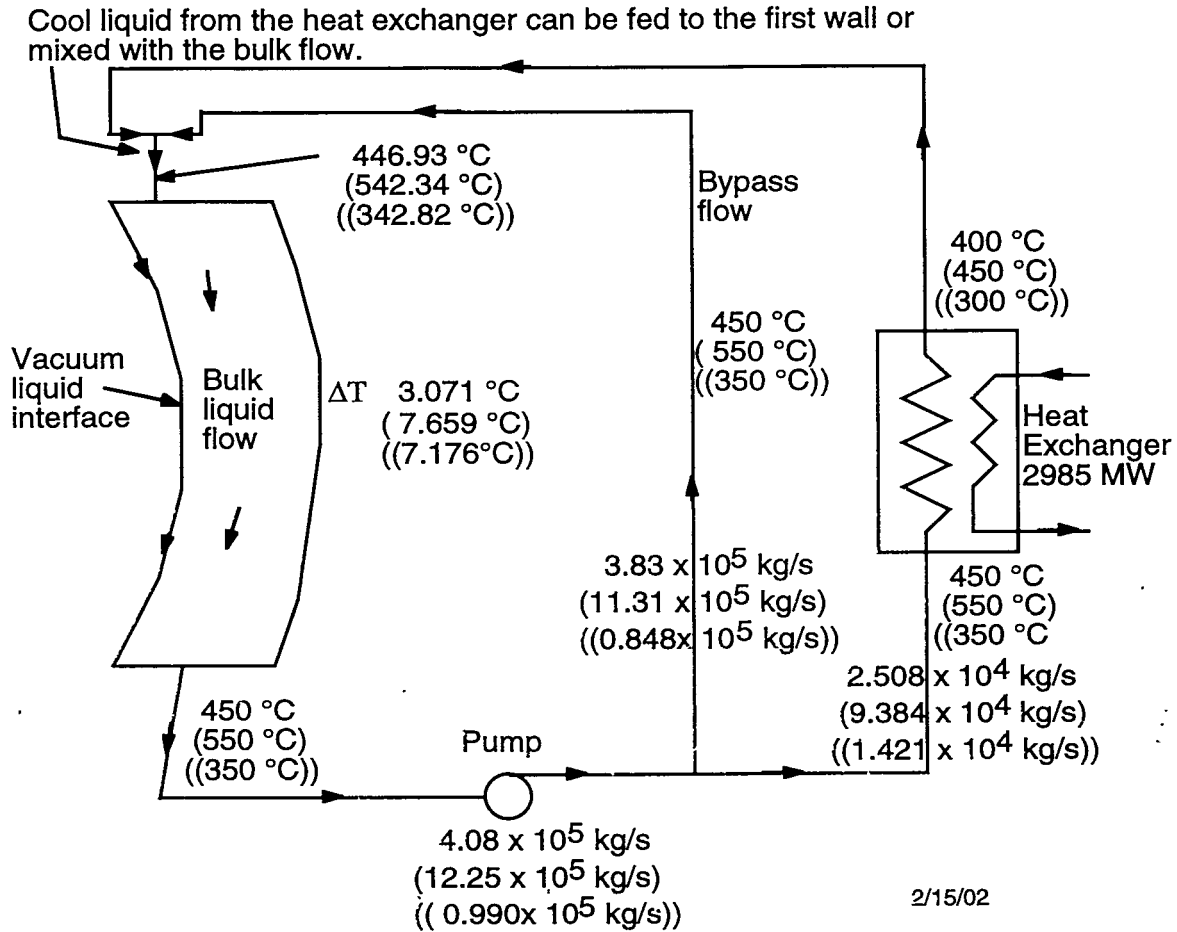

Fig 4. Mass flow and temperature diagram for flibe as the liquid wall. Numbers in parentheses are for SnLi and double parentheses are for Li.

Issues for flibe/flinabe case:

1-ΔT=50 °C across heat exchanger is low. There will be an economic penalty for having so low a value (100 °C is customary).

2-T_{cold} = 400 °C is close to the melt temperature, assumed to be 350 °C. Freeze-up will be an operational issue. Perhaps the melt temperature will be 310 °C and the temperature can be lowered somewhat.

3- T_{hot} = 450 °C is low for Carnot efficiency, so there will be an economic penalty (650 °C is customary).

Issues for SnLi case:

These seem reasonable from power plant point of view.

Issues for Li case:

1-ΔT=50 °C across heat exchanger is low. There will be an economic penalty for having so low a value 100 °C is usual).

2- T_{hot} = 350 °C is low for Carnot efficiency, so there will be an economic penalty (550 °C is customary for a liquid metal system).

Liquid wall design

The liquid flows in from the top in Fig. 1 with a nominal speed fo 10 m/s. In the case of flinabe there is enough azimuthal speed to keep the liquid on the outer wall by centrifugal force as shown by K. Gulec in related prior studies [Ref. 7, p 5-94 to 5-105]. In the case of SnLi and Li, we assume the magnetic field will keep the flow closely following field lines. Stability of liquid metal flow is an area needing study.

The bulk of the liquid is heated up mostly by neutrons by only 3° C for flinabe, 7.7° C for SnLi and 7.2° C for Li cases, as shown in Fig. 4. The radiation in the form of optical line radiation coming from the core interior and the edge plasma and bremsstrahlung radiation from the core heats the liquid near the surface. We need to know the surface temperature in order to calculate the evaporation rate.

We will treat two cases; one with relatively little optical radiation and one with enhanced optical radiation. The power flow to the divertor is highest with the lowest radiation to the wall case. We believe these two extreme cases will bracket the trade-off between a large wall evaporation and large divertor evaporation.
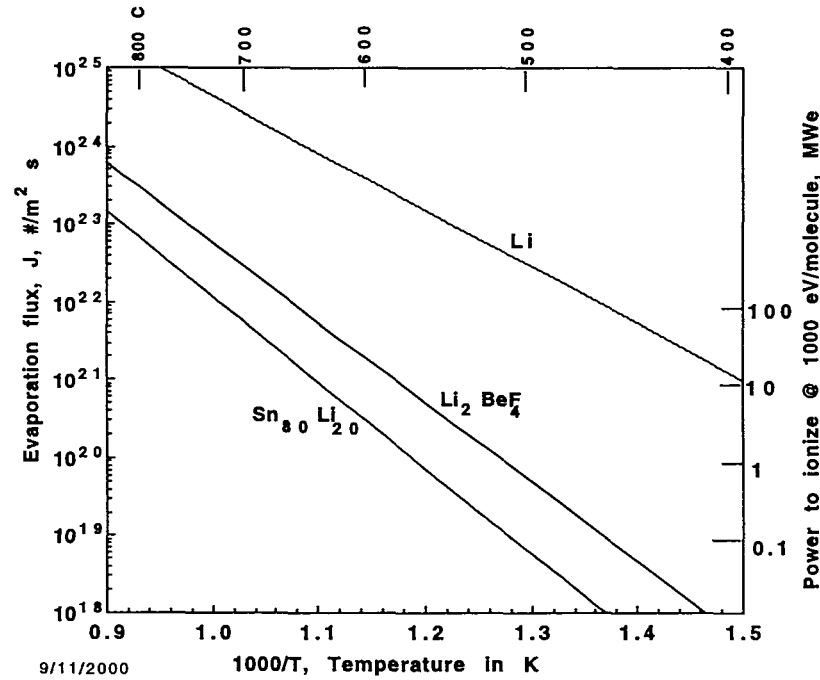
Fig. 5. Evaporation rates into vacuum for candidate liquids based on
Ref. 7 p 8-14 to 8-18. The values given are based on data at high
temperatures ~1000 °C and extrapolated to lower temperatures and
may be high, especially in the case of flibe.

The vapor pressure for Li_2BeF_4 used was $P(Torr) = 10^{9.00045-10441.05/T}$ from [10]
Cantor, Hsu and Ward (1965). At 500 °C, new theoretical analysis lowers this
predicted value by about a factor of two [11] (Olander, Fukuda, and Baes, Jr.,
2002). Adding NaF to flibe will lower the vapor pressure further due to dilution
of BeF_2 and allow operating at a lower temperature for the inlet liquid due to the
lower melt temperature of flinabe [5] (Peterson, 2001).

From Table 5, we see the low radiation case has 0.35 MW/m^2 of optical line
radiation surface heat load and 1.29 MW/m^2 in the high radiation case. The
Bremsstrahlung radiation for the flibe case was mistakenly left out of the
calculation. Inclusion will raise the film drop by the ratio of $0.45/0.35$. For SnLi,
the surface heat load is 0.48 MW/m^2 and 1.42 MW/m^2 for the low and enhanced
radiation cases. Photons of 10 keV penetrate ~ 1 mm into flibe, whereas the film
thickness is about 8 mm thick.

19

Table 5

Liquid wall power flux and temperature parameters

| Type of power | Low radiation | | | Enhanced radiation | |
	MW	MW/m²		MW	MW/m²
Brem	46	0.13		46	0.13
Line, core	75	0.21		280.2	0.774
Line, edge	50	0.14		186.8	0.516
Line, total	125	0.35		467	1.29
Charged power to divertor	454	3720 6 mm flux tube, one-ended		112	918 6 mm flux tube, one-ended
P_{total}, MW	625			625	
P_{rad}/P_{total}	0.27			0.82	
Flibe					
ΔT_{film}	27 °C			101	
$T_{surface}$	479 °C			553	
SnLi					
ΔT_{film}	83 °C			245 °C	
$T_{effecitive}$	610 °C			734 °C	

The high Reynolds number (highly turbulent) flowing liquid with a free surface has eddies at the surface causing the surface to undulate. The transverse motion at the surface causes mass transport and therefore enhanced heat transfer over pure conduction. As we move into the liquid, the eddies get larger and heat transfer is enhanced even more by convection. The equivalent thermal conductivity $k_{equivalent}$ has been calculated by Smolentsev [12], based on models discussed in [13] and plotted in Fig. 6 for flibe divided by the classical thermal conductivity k, for the flow speed of 10 m/s and 0.5 m thickness. We take k to be 1.06 W m^{-1} K^{-1}. Smolentsev gets an enhancement of thermal conductivity at the free surface of 100. At the back wall there is a 70 μm laminar layer with no transverse motion. Thus the enhancement is unity. We will assume flinabe and flibe have the same properties.
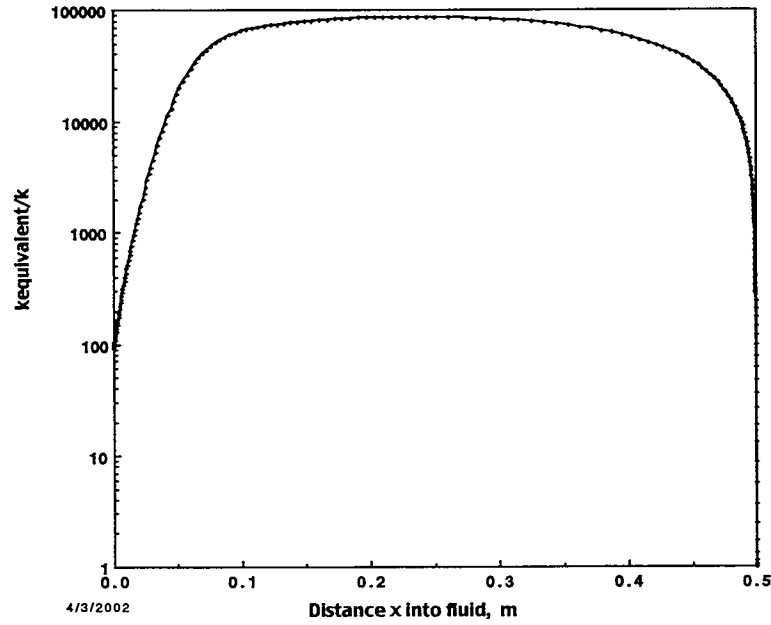
Fig. 6. Thermal conductivity for flinabe and flibe versus distance from the free surface into the flowing liquid.

We can get the temperature profile by integrating the heat conduction equation:

$$\frac{P}{A} = -k_{equivalent} \frac{dT}{dx} \tag{26}$$

Rearranging terms:

$$dT = -\frac{P}{k_{equivalent} A} dx \tag{27}$$

Integrating:

$$\Delta T_{film} = T(x=0) - T(x) = -\int_0^x \frac{P}{k_{equivalent} A} dx \tag{28}$$

The integral using the variable equivalent thermal conductivity, from Fig. 6 is plotted in Fig. 7.
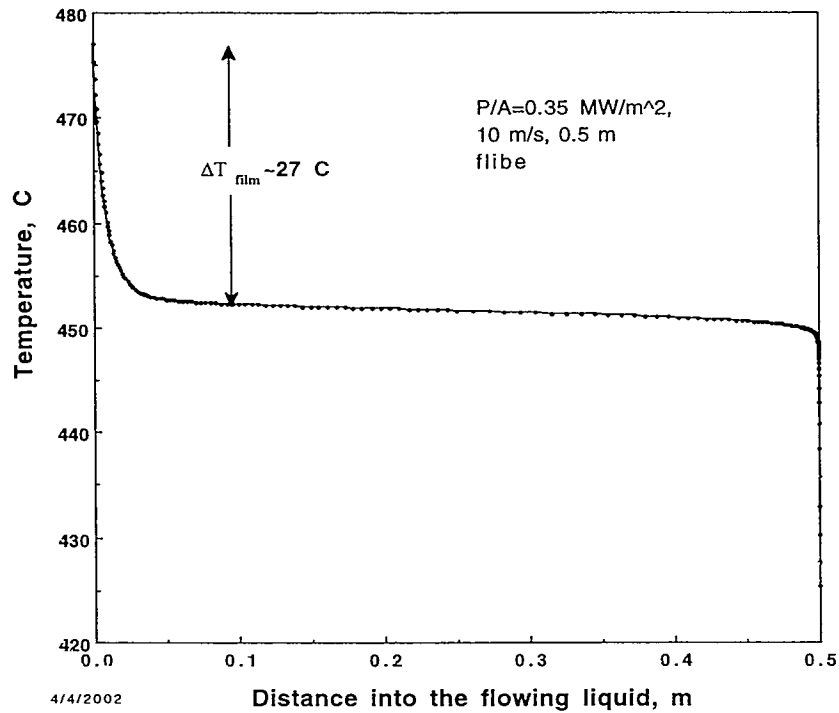
21

Fig. 7. Temperature profile through the flowing liquid.

There is a film drop on the surface and a flat temperature profile in the very turbulent interior and a film drop on the back wall, which we will ignore because there is very little heat removal there in our case. The heat is practically all convected out with the flow.

P/A=0.35 MW/m^2
10 m/s, 0.5 m
flibe

4/4/2002

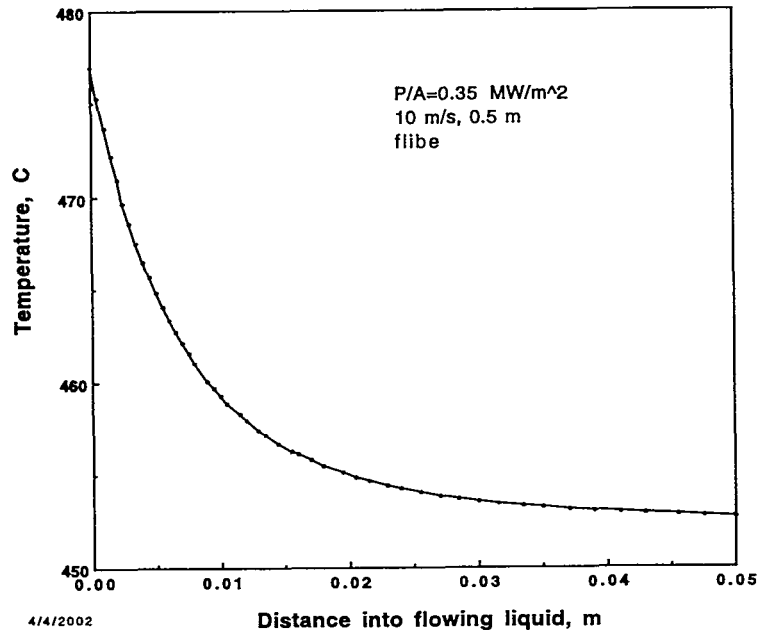Distance into flowing liquid, m

Fig. 8. Temperature profile near the free surface.

The temperature drop from the surface to the interior or bulk is approximately 27 °C for this case, with most of this drop occurring in a distance of 8.5 mm. We call this the surface film. It is seen in Fig. 7 & 8.

It may be useful to use the heat transfer coefficient, h, to calculate surface temperature.

$$\frac{P}{A} = h(T_{surface} - T_{bulk}) = h \Delta T_{film} \tag{29}$$

$$h = \frac{k_{equivalent}(x=0)\dfrac{dT}{dx}(x=0)}{\Delta T_{film}} \tag{30}$$

From Fig. 7 we get the film drop and from Fig. 8 we get the derivative at the surface.

$$h = \frac{106\,W/mK\,\dfrac{27K}{0.008m}}{27K} = 13,250\,\frac{W}{m^2 K} \tag{31}$$

For the liquid metal cases of SnLi and Li, we assume the motion is laminar and use the pure conduction temperature rise formula:

23

$$\Delta T_{film} \stackrel{\bullet}{=} 2\frac{P}{A}\sqrt{\frac{t}{\pi k \rho C}} \tag{32}$$

This equation gives the temperature rise as the surface moves along while being heated with a surface heat load of P/A, W/m^2. For our case, we take typically 10 m/s and 15 m of path length or 1.5 s of exposure. The exit temperature equals the entrance temperature + ΔT_{film} + $\Delta T_{blanket}$. Typically we have found the average evaporation occurs at a temperature about 3/4 of the way between the inlet and outlet temperature: Let us call this temperature the effective temperature, T_{eff}.

$$T_{eff} = T_{inlet} + \frac{3}{4}(\Delta T_{surface} + \Delta T_{blanket}) \tag{33}$$

$$\text{For flibe } T_{eff} = T_{inlet} + \Delta T_{film} + \frac{3}{4}\Delta T_{blanket} \tag{34}$$

Table 6

Summary temperatures for liquid walls

	Low radiation case			Enhanced radiation case		
	Flibe	SnLi	Li	Flibe	SnLi	Li
ΔT_{film}, °C	27	83	48	101	245	177
$T_{effective}$ °C (T-allowed from edge plasma analysis)	479 (520)	610 (630)	384 (410)	553 (520)*	734 (630)*	481 (410)*

*The edge plasma will be perturbed for the enhanced radiation case, so that new calculations will be needed.

The average evaporative flux from the wall for flinabe for the low radiation case at 0.35 MW/m^2 is 2×10^{19} m^{-2}s^{-1} and at the enhanced radiation case of 1.29 MW/m^2 is 5×10^{20} m^{-2}s^{-1}.

The average evaporative flux from the wall for SnLi for the low radiation case at 0.48 MW/m^2 is 8.9×10^{18} m^{-2}s^{-1} and at the enhanced radiation case of 1.42 MW/m^2 is 8.0×10^{20} m^{-2}s^{-1}. The inlet temperature was 542 C, and the exit temperatures for the two cases were 626 C and 787 C respectively.

The predicted temperature of the liquid wall due to heating from radiation is lower than the allowed temperature due to contamination from evaporation for the low radiation cases. However, it is higher for the enhanced radiation cases. This result is somewhat encouraging, depending on the amount of optical radiation.

Table 7

Properties used for candidate liquids

Liquid	C, J/kgK	ρ, kg/m3	k, W/mK
Flibe/flinabe	2380	1900	1.06
Li	4360	450	53*
SnLi	318	6000	40 *
PbLi	160	8700	15*
Ga	380*	5900	60*
Sn	230*	5700	35 *

*500 C°

Divertor design

The divertor is the region where the leakage plasma disposes of heat and particles and is shown in Fig. 1 (expanded view in Fig. 9). We plan to remove heat by injecting a high speed (up to 100 m/s) set of jets at a small angle to the magnetic flux which guides the plasma flow. The jets are shown in side- and end-views in Fig. 10. The jets can be made to form droplets if desired.
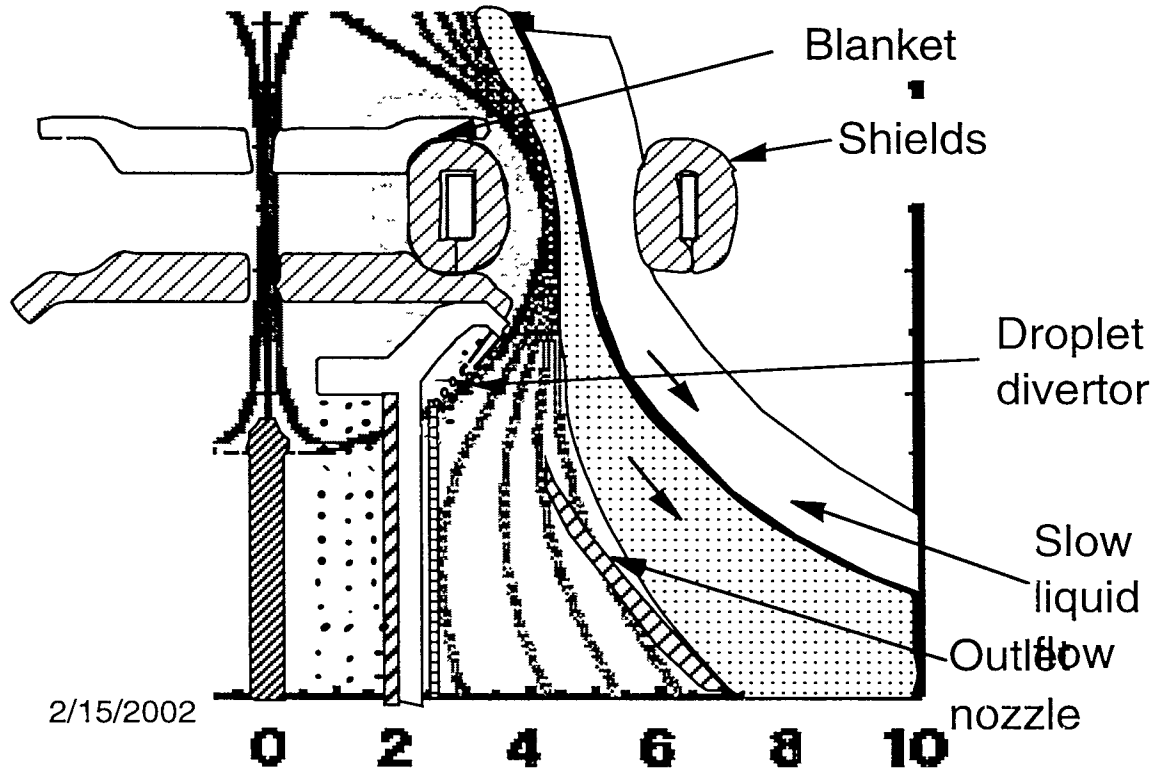
Fig. 9. The jets in the divertor are shown at 5° to the flux.

A vertical riser tube brings liquid up to an inner and outer spray nozzle. These nozzles spray many rows of small jets or droplets (~1 mm dia) to intercept the edge plasma. They carry away heat and provide surface area for condensation of evaporated droplet material. The insulator must be protected from direct particle bombardment either by a sufficiently dense droplet stream or a low conductivity film on the surface.
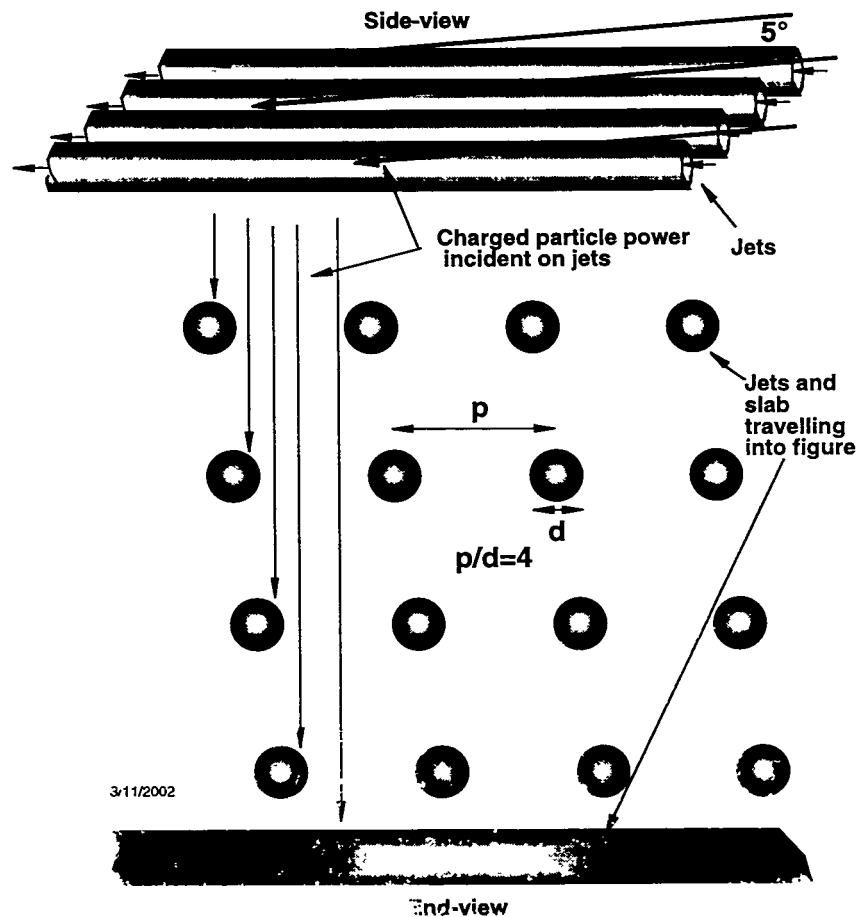
Fig. 10. Side and end-view of jets in the divertor are shown at 5° to the flux.

The distance at the midplane of the separatrix (r=0) and the secondary (inactive) separatrix (r=5.0015 m) is 1.5 mm. This flux tube at the jet diverto. becomes 6 mm (at r=3 m, z=-12 m). If the leaking plasma that passes across the separatrix were to completely fill this 1.5 mm flux tube, all the power would flow to the divertor at the bottom. However, the edge plasma, being diffusive, typically has a dimension an order of magnitude larger than this. Therefore, nearly equal amounts would flow out the top and through the aperture where the retractable electrode is shown in Fig. 1. The retractable electrode could be completely removed during normal operation after start-up. The plasma flowing through this aperture could go into a large tank with plenty of room to spread out the heat. This needs to be looked at in future design studies.

For the discussion to follow we are going to assume that the 6 mm wide flow into the bottom divertor takes all of the power and this dimension grows to 12 mm. The enhanced radiation case of 112 MW flowing into the one-ended divertor then produces a power density of 459 MW/m^2 over the 12 mm wide flux tube. If only half of the power flows is out the bottom, then the power density would drop in half to a somewhat more reasonable value of 229 MW/m^2 for a double-ended divertor. This change needs to be studied in future iterations of the design.

We now ask what are the evaporation rates for a liquid slab divertor and a jet divertor inclined at a small angle to the flow for a power density of 459 MW/m^2. The results for a slab inclined at 5° with a flow speed of 20 m/s are 1.09×10^{28} m^{-2}s^{-1} average flux for flibe and 2.64×10^{22} m^{-2}s^{-1} for SnLi. T_{in} = 673 K and T_{out} = 2383 K for flibe and T_{in} = 673 K and T_{out} = 1107 K for SnLi. T_{in} for SnLi should have been 723 K for consistency with the fluid to the divertor from the cold leg of the heat exchanger. For four rows of jets (p/d=4) followed by a slab as shown in Fig. 11, the analysis shows a reduced evaporation. The results are 3.64×10^{23} m^{-2}s^{-1} for flibe and 4.82×10^{18} m^{-2} s^{-1} for SnLi. The surprising reduction of them evaporative flux is due to the reduction by a factor of 3.14 in average power. Circulation in the jets, exposing all sides to the incident power, results in a factor of 3 lower temperature rise. The surface temperature appears in the exponent of the evaporation equation.

For the low radiation case, the charged power to the divertor of 454 MW over a 12 mm wide flux tube would result in 1860 MW/m^2. The evaporation with 100 m/s jet speed is estimated at 6.0×10^{25} m^{-2}s^{-1} for flinabe and 1.4×10^{20} m^{-2}s^{-1} for SnLi.

Edge plasma analysis

The plasma beyond the magnetic separatrix shields the core plasma from the impurities that evaporate from the liquid wall. Here we discuss the modeling of this scrape-off layer (SOL) plasma and present results on the effectiveness of the shielding. With respect to the liquid first-wall, the maximum flux of impurities that the SOL plasma can shield then determines the allowable surface temperature of the liquid. The surface is heated by a combination of bremsstrahlung and line radiation from the core and edge region (see Table 2). The heat flux to the divertor region is also important, because it defines what peak heat flux must be tolerated by the divertor.

The initial model for the edge plasma considers the thin annulus of the edge region as a long-thin plasma slab. The X-points are taken to be 10 m apart, and a divertor leg region of 2 m is used at each end. Because the toroidal magnetic field at the edge of a spheromak is small compared to the poloidal field, we take the B-field to have only a poloidal component. We assume that the divertor leg regions can be designed to give low-recycling of the hydrogen plasma, perhaps by drawing these field lines into a large dump tank. Thus, the hydrogenic recycling coefficient at the divertors is assumed to be $R_h=0.25$. At the separatrix density of the hydrogenic species (a 50/50% mixture of deuterium and tritium) is taken to be 5×10^{19} m^{-3} and power into the SOL is taken as 0.6×10^6 W/m^2 in both the ion and electron channels. The anomalous radial diffusion coefficients arising from plasma turbulence is 0.33 m^2/s for density, and 0.5 m^2/s for electron and ion thermal energies.

The calculated radial plasma profiles at the outer midplane are shown in Fig. 11. The scale length of the density, n_i and electron temperature, T_e, are very similar with a 1/e value of 0.8 cm. The ion temperature has a characteristic high-temperature tail because the ion parallel thermal conductivity is much lower than that of the electrons. This allows radial diffusion to be substantial.
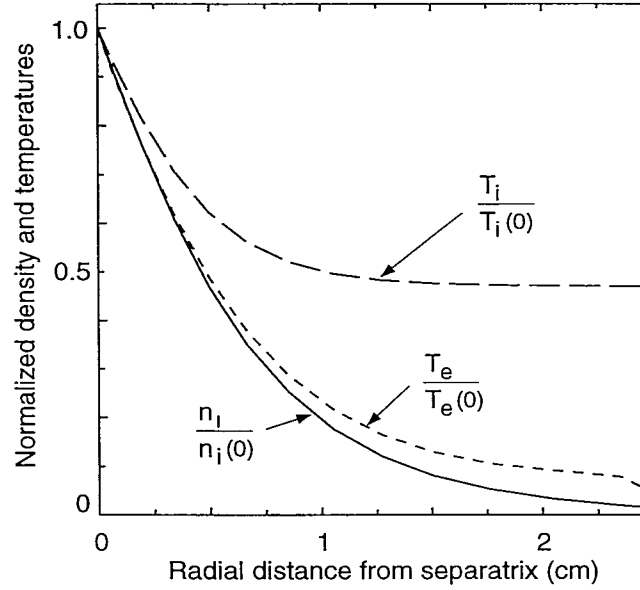
29

Fig. 11. Radial profiles of ion density, and electron and ion temperatures. Values at the separatrix are $n_i(0)=5\times10^{19}$ m^{-3}, $T_e(0)=493$ eV, and $T_i(0)=504$ eV. The input power from the core is 1.2×10^6 W/m^2.

The impurity gas coming from the liquid wall is modeled as a uniform flux along the radial boundary at r=6.025 m (which is 2.5 cm beyond the separatrix edge) at a temperature of 1 eV [14] (Rognlien, 2002?). The impurities have the same anomalous radial diffusion coefficients as the hydrogenic species. The impurity ions that return to the side wall and those reaching the divertor plate through axial flow are assumed to be reabsorbed mostly into the liquid with a small recycling coefficient of $R_{imp}=0.25$. Values of $R_{imp}<0.5$ produce very similar results. We consider two impurity gas species, lithium and fluorine. Lithium is from either a pure lithium wall or from a tin-lithium wall, which evaporates nearly all lithium. The second impurity gas considered is fluorine, which comes from the molten salts flibe or flinabe. Because fluorine has the highest charge of the atoms in these salts, it has the lowest allowable concentration at the core edge. The resulting impurity concentrations at the core edge are shown in Fig. 12.
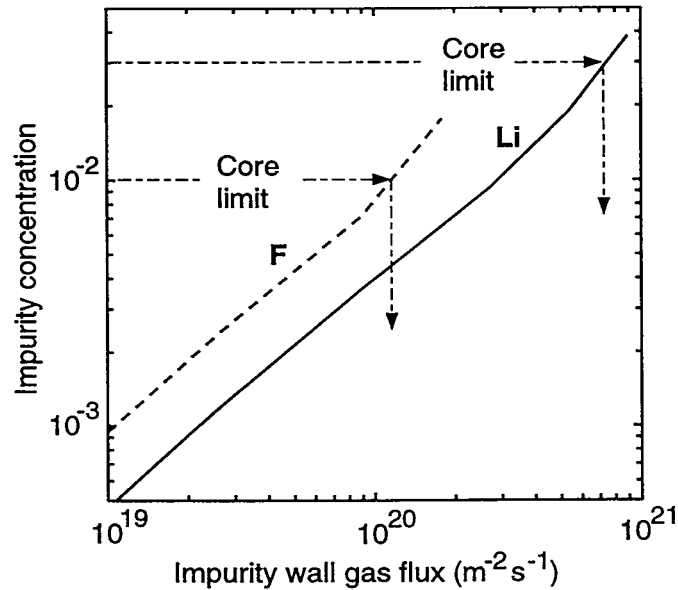
Fig. 12. Concentration of impurities (n_{imp}/n_e) at the separatrix for various liquid wall impurity gas fluxes distributed uniformly along the wall located 2.5 cm outside the separatrix.

Data from the vapor pressure of the various liquids versus temperature (see Fig. 5) is then used with a simple model to calculate the vapor flux. Using the limits of flux noted in Fig. 12, we arrive at the following wall temperature limits for three materials:

Table 8.

Maximum surface temperatures of liquid walls

based on acceptable core impurity levels.

Material	Lithium	Tin-lithium (80/20)	Flinabe/Flibe
Surface Temp. °C	410	630	520

The heat flux at the divertor plate is very large in this simple slab model that does not include any expansion of the magnetic flux surfaces shown in Fig. 1 & 9. For the cases considered here, the parallel heat flux is equal to the poloidal heat flux, because there is no toroidal B-field. As a consequence, the flux is

31

approximately 1 GW/m². The flux expansion of ~10:1 will reduce this to ~100 MW/m² This model is double-ended, i.e., double-null. The area of the flux tube before expansion at the 3 m radius divertor is $2 \pi 3$ m x 0.008 m = 0.151 m². The escaping power is 454 MW from Table 5 giving 454 MW/0.151 m² x 0.5 (two-ended) = 1500 MW/m². If this flux tube expanded to 12 mm as discussed earlier the power density would be 1500 x 8/12 = 1000 MW/m².

The temperature limit of the divertor surfaces is set by sputtering and evaporation. The latter limit involves the sheath superheat phenomenon as studied for tokamaks [15, 16]. Based on those studies a rough evaporation-based limit for the present purposes is set by the condition that the evaporating impurity flux is approximately equal to the incoming hydrogen ion flux [15, 16]. This flux ratio is, "G" = (impurity atom flux)/(hydrogen ion flux). When G >> 1, (exact limit depending on surface material, flow velocity, and plasma paramters) the sheath collapses and runaway overheating of the surface occurs. For our base-case of a low-recycling divertor, the peak hydrogen ion flux is 2×10^{24} $\sin\theta_\tau$ particles/m² s, where θ_τ is the tilt angle that the divertor stream makes with the B-field; $\theta_\tau = 5°$ for the design here. Thus, the rule of G=1 implies that the maximum impurity flux is 2×10^{23} (particles/m² s). From curves of evaporative flux versus surface temperature for different materials shown in Fig. 5, such a flux corresponds to the following temperatures: for Li, T=580 °C; flibe/flinabe, T=740 C; for SnLi, T=840 C, and for Sn, T=1380 C. (For lithium, the sputtering limit is likely to be more restrictive). These results can be compared to those predicted on p 28 from heat transfer. For flibe, the evaporative flux predicted from heat transfer with rotating jets was 3.6×10^{23} (particles/m² s) for the high radiating edge case. Perhaps this case is workable. For the low radiating edge case, the evaporative flux is about two orders of magnitude larger and seems unworkable. Clearly, this subject needs more study.

For our base-case, the divertor surface is heated by a peak heat flux of 1×10^3 $\sin\theta_\tau$ (MW/m^2) with a width of $0.6/\sin\theta_\tau$ (cm). The peak temperature of the surface then depends on the conductivity of the liquid, which can be considerably enhanced by any turbulence, especially for low conductivity molten salts flibe and flinabe. Such an analysis is described in section, **Liquid Wall Design.**

Tritium breeding analysis

Potential for tritium breeding was assessed in the spheromak shown in Figure 1. The radial blanket consists of 50 cm thick fast-flowing liquid layer followed by ~50 thick slow-flowing liquid layer. Flinabe is considered in the present assessment, but a comparison of the adequacy of tritium breeding is also made for Flibe. A design goal is to eliminate the presence of any neutron multiplier (e.g. beryllium) other than that already in the liquid in the radial blankets shown in figure 1 due to its limitation on radiation damage lifetime, and complexity as well as resources concerns. However, the top and bottom blankets could be designed to be dedicated regions to supplement any additional tritium such that tritium self-sufficiency is achieved in the spheromak with a possibility of utilizing beryllium as a multiplier in these regions. Geometrically, the top and bottom regions occupy ~7.5% each, of the 4π of the solid angle, while the radial blanket covers the remainder (~85%).

Table 9 shows the options considered in the present assessment. It was shown that lithium-6 enrichment of 50% or higher is needed with flinabe, while enrichment of ~25% is adequate in the flibe case.

Table 10 gives the total tritium breeding ratio (TBR) and the contribution from each blanket when Flinabe is considered as the liquid breeder (design option I). As shown, without beryllium in the top and bottom blankets, the TBR is marginal (TBR ~1.05). There is a risk that TBR may fall below unity if more accurate calculations (3-D) and accounting for present nuclear data uncertainties

33

are made. The TBR improves upon the utilization of a front Be zone in the top and bottom blankets. In this case, a TBR with comfortable margin is achieved. The TBR is ~ 1.12 when 10 cm thick beryllium zone is used in the top and bottom blankets and is ~1.15 with 20 cm thick Be zone.

Table 11 gives the corresponding tritium breeding capability in case the Flibe (25% Li-6) is used instead. The TBR is larger than with Flinabe by ~11-13% (with Be in top and bottom blankets) and by ~15% (with no Be in top and bottom blankets).

Design option III (using Li-Pb in the top and bottom blankets while Flinabe (or Flibe) is used in the radial blanket) does not offer significant improvement in TBR, as shown in Table 12.

Table 9
Options Considered in Evaluating Tritium Breeding

	Option I	Option II	Option III
Radial Blanket (No Beryllium)	Flinabe (50% Li-6)	Flibe (25% Li-6)	Flinabe or Flibe
Top Blanket	Flinabe (50% Li-6)	Flibe (50% Li-6)	Li-Pb (90% Li-6)
Bottom Blanket	*No Beryllium* *10 cm Be zone* *20 cm Be Zone*	*No Beryllium* *10 cm Be zone* *20 cm Be Zone*	

Table 10
Total TBR with Flinabe and Contribution from Various Blankets
(Option I)

Blanket Location	TBR	Contribution
Radial Flinabe Wall/Blanket (No Beryllium)	0.897	~85%[1] ~80%[2] ~78.3%[3]
Top Flinabe Blanket		
No Beryllium	0.078	~7.5%
10 cm Be Zone	0.111	~10%
20 cm Be Zone	0.124	~10.8%
Bottom Flinabe Blanket		
No Beryllium	0.078	~7.5%
10 cm Be Zone	0.112	~10%
20 cm Be Zone	0.125	~10.9%
Total TBR		
No Beryllium	*1.05*	
10 cm Be Zone	*1.12*	
20 cm Be Zone	*1.146*	

1 No Be in Top and Bottom Blankets

2 10 co Be zone in Top and Bottom Blankets

3 20 cm Be zone in Top and Bottom Blankets

Table 11

Total TBR with Flibe and Contribution from Various Blankets

(Option II)

Blanket Location	TBR	Contribution
Radial Flibe Wall/Blanket (No Beryllium)	1.032	~85%[1] ~81.5%[2] ~80.6%[3]
Top Flibe Blanket		
No Beryllium	0.089	~7.5%
10 cm Be Zone	0.118	~9.3%
20 cm Be Zone	0.124	~9.7%
Bottom Flibe Blanket		
No Beryllium	0.089	~7.5%
10 cm Be Zone	0.117	~9.2%
20 cm Be Zone	0.125	~9.7%
Total TBR		
No Beryllium	*1.21*	
10 cm Be Zone	*1.267*	
20 cm Be Zone	*1.281*	

1 No Be in Top and Bottom Blankets

2 10 co Be zone in Top and Bottom Blankets

3 20 cm Be zone in Top and Bottom Blankets

Table 12

TBR with Flinabe or Flibe Breeder in Radial Blanket
And LiPb in Top and Bottom Blankets (Option III)

Blanket Location	TBR	Contribution
Radial Blanket (Flinabe)	0.897	~80.8%
Radial Blanket (Flibe)	1.032	(~82.8%)
(No Beryllium)		
Top LiPb Blanket	0.107	~9.6%[1]- ~8.6%[2]
Bottom LiPb Blanket	0.107	~9.6%[1]- ~8.6%[2]
Total TBR: *With Flinabe*	*1.111*	
With Flibe	*1.246*	

1: With Flinabe in Radial Blanket...... 2: With Flibe in Radial Blanket

Conclusions and discussion

This study examines a steady-state spheromak with a flowing liquid wall. We are sufficiently encouraged by the results to recommend further work on the concept. However, for flibe, the evaporation from the walls in the high radiating edge case is too high, and for the low radiating edge case, the divertor evaporation is too high. The advantages of the simpler reactor embodiment of the spheromak (without toroidal coils and liquid walls replacing most of the solid first wall) are impressive.

Inconsistencies needing resolution or improved performance are:

- Evaporation from the walls exceed the allowed value for the enhanced radiation case but seems acceptable for the low radiation case. The bremsstrahlung radiation needs to be added to the wall heat load for the flibe case to get a revised film temperature drop estimate. Better estimates of

optical radiation are needed. The film drop used 0.35 MW/m^2 rather than 0.48 MW/m^2, as it should have been. The evaporation in the divertor seems possibly acceptable for the high radiating edge case but not for the low radiation edge case.

- The scrape-off layer plasma (~10 mm) exceeds the magnetic flux layer of 1.5 mm, thus the assumption that most of the exhaust goes to the single null divertor at the bottom is not achieved. The vertical scrape-off layer can exit the machine through the small aperture at the top into a large open tank. This may be a big advantage by lowering the power density in the divertor.

- The gun threading magnetic flux is unusually small (1/1000 time the spheromak flux). Will this be realistically achievable?

- The plasma parameters need to be estimated more accurately with more detailed modeling.

- We should learn how to breed tritium without enriching the lithium and without adding solid beryllium to the blankets at the top and bottom.

Acknowledgments

References

1. P. M. Bellan, Spheromaks, Imperial College Press, London, 2000.

2. R. L. Hagenson and R. A. Krakowski, Fusion Techn. 8, 1606 (1985).

3. L. J. Perkins, unpublished work on spheromak reactor designs (1995).

4. T. K. Fowler, D. D. Hua, E. G. Hooper, R. W. Moir and L. D. Pearlstein, Pulsed spheromk fusion reactors," Comments on Plasma Physics and Controlled Fusion, Comments on Modern Physics, Vol 1 Part C 83-98 (1999)

5. P. F. Peterson, UC Berkeley, private communications in a briefing (March 4, 2001).

6. T. K. Fowler and E. B. Hooper, "Advanced Spheromak Fusion Reactor", submitted to the 8th International Conference on Emerging Nuclear Energy Systems (Obninsk, Russia) June 24-28, 1996. Lawrence Livermore National Laboratory Report UCRL-JC-124363, June 19, 1996.

7. M. A. Abdou et al. "On the exploration of innovative concepts for fusion chamber technology," UCLA-ENG-99-206 (1999). Fusion Engineering and Design **54** (2001) 181-247.

8. T. K. Fowler, D. D. Hua and B. W. Stallard, "Simulations of SSPX Sustainment -- Toward a Standard Model for Spheromaks," UCRL-ID141998, Jan. 12, 2001.

9. C. W. Barnes, T. R. Jarboe, G. J. Marklin, S. O. Knox and I. Henins, Phys. Fluids B **2**, 1871 (1999).

10. S. Cantor, D. S. Hsu, and W. T. Ward, "Vapor Pressures of Fluoride Melts," in Reactor Chem. Div. Ann. Progr. Rept., Oak Ridge National Laboratory, Oak Ridge, Tenn., ORNL-3913, pp. 24-26 (1965). For Flibe.

11. D. R. Olander, G. Fukuda, D. F. Baes, Jr. (2002), "Equilibrium Pressures Over BeF_2-LiF (Flibe) Molten Mixtures," Fusion Science and Technology 41(2):141-150.

12. S. Smolentsev, UCLA, private communications, November 13, 2001.

13. S. Smolentsev, M. Abdou, N. Morley, A. Ying, T. Kunugi, "Applications of the "K-ε" model to open channel flows in a magnetic field," Int. J. Engineering Science, In press (2002).

14. T. D. Rognlien, (2002).

15. J.N. Brooks and D. Naujoks, "Sheath superheat transmission due to redepositon of thermally emitted material," Phys. Plasmas, Vol. 7 (2000) 2565.

16. D. Naujoks and J.N. Brooks, "Combined sheath and thermal analysis of overheated surfaces in fusion devices," J. Nucl. Mater., Vol. 290-293 (2001) 1123.